Maximum Output Power Point Tracking for Low Power Photovoltaic Energy Harvesting Systems

L. Vicente-García, Ó. Pereira-Rial, P. López
Centro Singular de Investigación en Tecnoloxías Intelixentes (CiTIUS)
Universidade de Santiago de Compostela
Santiago de Compostela, Spain

***Abstract*—A novel approach for finding the maximum output power point of a photovoltaic energy harvesting system is proposed in this paper. It is based on maximizing the power delivered to the load taking into account the performance of the whole system in contrast to conventional approaches focused on tracking the maximum power point of the photovoltaic transducer alone. The output power tracking is performed by measuring the output voltage, which significantly simplifies the hardware complexity and consequently reduces the power consumption. A circuit implementation of the entire system is presented and validated using electrical simulations. The designed circuit is self powered and is able to successfully supply a load with voltage levels higher than 1.2V. The system achieves a peak efficiency of 80.51% when the input power is equal to 28.03 µW.**

***Index Terms*—Energy harvesting, MPPT, DC-DC converters**

I. Introduction

Biomedical implantable and wearable devices play a key role in modern therapy and diagnosis [1]. Depending on the application, the consumed power of these devices ranges from microwatts to milliwatts [2]. The hazardous nature of batteries, their size, lifespan and the need for surgical replacement make energy harvesting an appealing alternative for powering these devices. Light energy harvesting, on the other hand, has greater harvesting power density than other environmental sources [3] and has already been demonstrated as a viable solution in low power biomedical applications such as intraocular pressure monitoring [4] and subdermal implants [5].

Maximizing the power delivered to the load circuit is a key feature of any energy harvesting system. In the particular case of photovoltaic sources this is usually done by monitoring the power versus voltage curve of the photovoltaic cell and setting the system's operating point at the curves's maximum power point, the so-called Maximum Power Point Tracking (MPPT) technique, [6]. Traditional approaches to MPPT are therefore oriented to force the circuit's operation to the point of highest available input power. However, the other elements present in the energy harvester circuit (essentially, the DC-DC converter) will influence the final harvested power and should be taken into account. As we will show in this work, forcing the system to operate at the point at which the photodiode generates its maximum power might not be optimal from the point of view of the overall system performance, and there might exist a point of operation that lead to a higher output power. The aim of this work is to demonstrate this fact by using a mathematical model of a light powered energy harvester. Additionally, a transistor level implementation of a harvester circuit that maximizes the output power instead of achieving the MPPT of the light transducer is also proposed. The circuit was implemented and simulated in a commercial CMOS 180 nm technology, being able to autonomously harvest power from photovoltaic sources in the power range of µWs and voltage levels above 600 mV. The system exhibits a peak efficiency of 80.51%, yielding an output power of 22.56 µW, which makes it suitable for low power applications.

The work is organized as follows: in Section II, a mathematical equivalent model for both the photodiode and the DC-DC converter are given, which will be used to analyze the impact of the different parameters on the output power. A circuit implementation of a system that maximizes its output power is proposed in Section III and its functionality is demonstrated by simulation in Section IV. Finally, the conclusions of the work are drawn in Section V.

II. Mathematical Model

A simplified model of a photovoltaic energy harvester is shown in Fig. 1. The system is composed of a photodiode and a Power Management Unit (PMU), whose main block is a DC-DC converter. In this section, the impact of the different system parameters on the output power will be analyzed. To do so, the cross-coupled voltage doubler, a widely used charge pump (CP) topology for energy harvesting applications is considered. This type of converter is suited for energy harvesting applications due to its efficiency and integration capability. The output power of a cross-coupled voltage doubler based CP of N stages can be expressed as [7]:

$$P_{out} = (N+1)V_{in}I_L - I_L^2\frac{N}{2fC_{fly}} \tag{1}$$

where V_{in} is the input voltage, I_L is the load current, C_{fly} represents the pumping capacitor and f is the clock frequency.

This project has received funding from the Spanish Ministry of Science, Innovation and Universities under grant PID2021-128009OB-C32 and from Xunta de Galicia-Consellería de Cultura, Educación e Universidade Accreditation 2019-2022 ED431G-2019/04 and Reference Competitive Group Accreditation 2021-2024 ED431C2021/048, co-funded by (ERDF/FEDER programme).

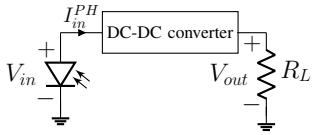

Fig. 1: Simplified model of a solar energy harvester.

The explicit dependence on I_L can be suppressed by taking into account that $V_{out} = I_L R_L$ and $P_{out} = V_{out} I_L$. After some manipulations, the following expression is obtained:

$$P_{out} = \frac{[(N+1)2fC_{fly}]^2 \cdot R_L}{(N+2fC_{fly}R_L)^2} \cdot V_{in}^2 \tag{2}$$

One could say that maximizing the input voltage and the clock frequency means maximizing the output power of the charge pump. However, additional considerations must be taken into account. First, a real implementation of a charge pump has some static losses, P_{sta}, which are increased when the input voltage increases ($P_{sta} \simeq c_{sta} V_{in}^2$, where c_{sta} is a constant, [7]). In addition, the dynamic losses, P_{dyn}, due to the charge/discharge of the nodes in an electric circuit, depend on the frequency of operation ($P_{dyn} \simeq C_p f V_{in}^2$, where C_p represents the parasitics). The analysis is further complicated when a non-constant supply source is taken into account.

In particular, when the power source is a photodiode, the input current provided to the PMU, Fig. 1, can be modeled using the following expression:

$$I_{in}^{PH} = I_{ph} - I_S(e^{V_{in}/nV_T} - 1) \tag{3}$$

where I_{ph} is the photogenerated current, I_S is the reverse saturation current of the photodiode, V_T the thermal potential and n the ideality factor.

A system composed of both the photodiode and the charge pump will operate at the point where the current provided by the photodiode, I_{in}^{PH}, is equal to that sinked by the charge pump, I_{in}^{CP}. For that reason, an expression for the input current of the converter is obtained next. The most relevant power losses of a CP can be expressed as:

$$P_{loss} = fC_p V_{in}^2 + I_L^2 \frac{N}{2fC_{fly}} + V_{in}^2 c_{sta} \tag{4}$$

Then, the total input power to the charge pump can be written as the sum of the output power and the power losses, $P_{in} = P_{out} + P_{loss}$. Making $I_{in}^{CP} = P_{in} V_{in}$ and using (1), the following expression can be obtained for the input current to the charge pump:

$$I_{in}^{CP} = (N+1)I_L + C_p f V_{in} + V_{in} c_{sta} \tag{5}$$

Once again, by suppressing the explicit dependency on I_L, the following equation is obtained:

$$I_{in}^{CP} = \left(\frac{2fC_{fly}(N+1)^2}{(N+2fC_{fly}R_L)} + C_p f + c_{sta} \right) V_{in} \tag{6}$$

The system is going to operate on a point where (3) equals (6). This equation cannot be analytically solved, although some iterative methods have been proposed, [8]. However, by simple inspection of these equations, it can be seen that for a given photodiode's curve, in order to change the point of operation some of the parameters of the converter must be changed. The most commonly tuned parameter is the frequency of operation. If we want the system to work on a fixed point (traditionally we would aim for the MPP), the charge pump would have to adapt its parameters to it, for example, by working at a certain frequency. However, this adaptation may not be the optimum one in terms of output power, and there might exist other operating points which lead to a higher output power.

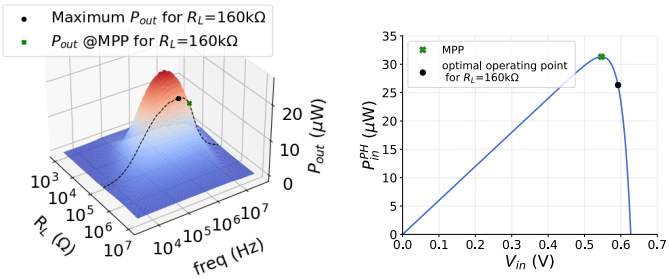

(a) (b)

Fig. 2: Representations of the (a) output power dependency with frequency and R_L and (b) points of operation over the photodiode's power curve for the particular case considered

To illustrate this point, Fig. 2a shows the dependency of the output power with the frequency and load resistance for a system with the following parameters: I_{ph} = 60 µA, I_S = 2 fA, N = 2, C_{fly} = 200 pF, C_p = 0.1·C_{fly} and c_{sta} = 0.2 µS. This graph was obtained using equations (2), (3) and (6) and solving them using numeric methods. For a particular case where R_L = 160 kΩ (dashed line in Fig. 2a), the maximum output power is achieved when working with a frequency of 957 kHz. If we analyze where this point of operation is located over the photodiode's power curve (Fig. 2b), it can be seen that it is not placed at the MPP. Choosing a different R_L will change the position of the point of operation that leads to a higher output power, but generally it will not coincide with the MPP of the light transducer.

III. Circuit Description

Taking into account the previously exposed results, a photovoltaic energy harvester that maximizes its output power has been designed in standard 180 nm CMOS technology. Some authors have successfully implemented harvesters that use this approach [9], but the tracked variable is the output current, which increases the circuit complexity. The proposed system only takes measurements of the output voltage, since maximizing the output voltage of a charge pump is equivalent to maximizing the delivered power if a constant load resistance is assumed. In order to perform this maximization, the system is provided with a control unit that performs the well-known *perturb and observe* algorithm [6]. The control unit makes perturbations in the frequency of operation and evaluates

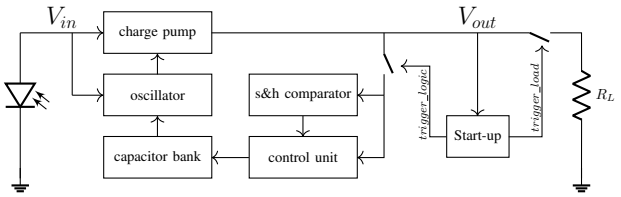

Fig. 3: Architecture of the proposed energy harvester.

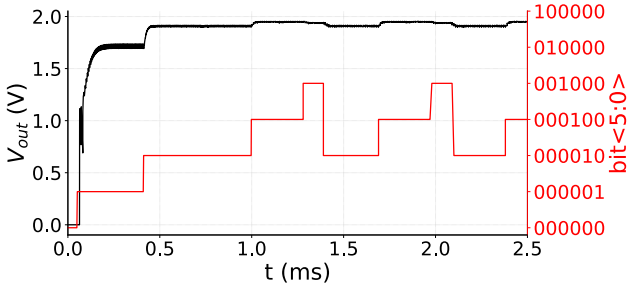

Fig. 4: Evolution of the output voltage (left axis) and active bit of the capacitor bank (right axis) under the action of the proposed algorithm for the particular case where $I_{ph} = 60$ µA and $R_L = 170$ kΩ.

their effect on the output voltage, choosing the direction of perturbation that leads to a higher voltage.

Fig. 3 shows the block diagram of the proposed system. It consists of a charge pump, an oscillator, a capacitor bank, a sample&hold comparator, a control unit and a start-up mechanism. The detailed description of the blocks is as follows:

1) Charge Pump: The chosen architecture is based on the well-known cross-coupled voltage doubler topology. In order to obtain a better driving capability [10], boosting techniques are implemented. The clock signals are boosted following the strategy described in [11], and the resulting boosted signals are used to generate the voltages that drive the gates of the switching transistors. Two stages are used, so an open loop voltage gain of 3 is expected.

2) Oscillator: It generates the clock signals in the system, i.e., the signals driving the charge pump switches and the clock used by the control unit. The structure chosen for the oscillator is the one proposed in [12]. The size, efficiency and accuracy of this topology make it suitable for energy harvesting applications. The oscillation frequency is controlled by modifying the capacitance of the oscillator (frequency is inversely proportional to capacitance). The capacitance is modified by using a capacitor bank consisting of several capacitors with different capacitance values that can be connected or disconnected through switches. The sizes of the capacitors have been chosen so that the resulting frequencies define clearly distinguishable regions of operation. The signals that control the switches are provided by the control block. The implemented system contains 6 capacitors in the capacitor bank and therefore, a 6-bit length digital word is used to control the frequency of operation.

3) Sample&Hold and comparator: To evaluate whether the voltage of the perturbed state is greater or lower than the unperturbed one, a S&H structure and a conventional dynamic comparator [13] are used. The sample and hold structure stores both output voltage values in two capacitors and then they are driven to the comparator to evaluate which frequency leads to a higher output voltage. The signals to control the storing process and enable the comparator come from the control unit.

4) Control Unit (CU): It generates the signals that control the comparator and, depending on the comparison result, tunes the frequency of the oscillator through the capacitor bank. This block is powered by the output voltage of the charge pump. For this reason, to achieve normal operation of the system, it is necessary to implement start-up mechanisms.

5) Start-up: It generates the signals that control the two switches shown in Fig. 3 that connect or disconnect the control block, the comparator and the load to/from the output of the charge pump. This is done using two level detectors (LD) based on the topology in [14]. These level detectors provide an output voltage equal to 0 when V_{out} is below a certain threshold and equal to V_{out} otherwise. Initially, while $V_{out} < 1$ V, the oscillator and the charge pump operate without connecting the load and with the control unit and the comparator turned off. Once $V_{out} \geq 1$ V, $trigger\_logic$ is activated and the control unit and the comparator starts to operate. When $V_{out} \geq 1.2$ V, $trigger\_load$ is activated and therefore, the load is connected to the output of the charge pump and the whole system achieves the normal operation mode. When either the control block or the load is connected to the output of the charge pump, a voltage drop is expected. Because of this, to avoid stability issues, the level detectors were implemented including hysteresis.

IV. Simulation Results

Transient transistor-level simulations have been conducted to check the correct functionality of the system. Fig. 4 shows an example of the system's behavior under the algorithm's action for a particular case where $I_{ph} = 60$ µA and $R_L = 170$ kΩ. During start-up, the control block is not being powered and none of the switches of the capacitor bank is activated. For that reason, an auxiliary capacitor of 1 pF that sets a default frequency of 50 kHz was implemented. Under these conditions, the start-up only lasts 63 µs. Once the output voltage of the charge pump is high enough to power the control block and the comparator, the algorithm's action starts. Consecutive perturbations and comparisons are carried out during the entire time of operation. The oscillator begins with bigger capacitances, which correspond to lower frequencies, and the control unit progressively lowers them, increasing the frequency. The range of frequencies the system is able to provide spans from 100 kHz to 3 MHz. Initially, increasing the frequency makes the output voltage rise as well. However, when the frequency exceeds a certain value (the digital word 001000 in Fig. 4, which corresponds to a frequency of 700 kHz), the output voltage decreases. Comparison results

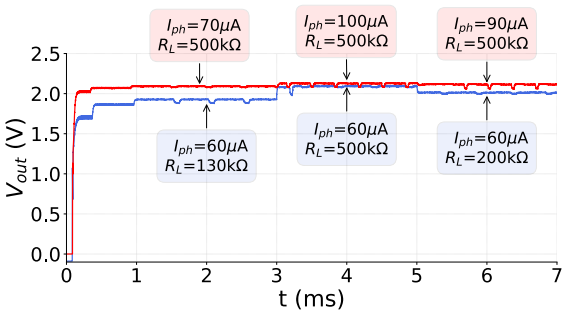

Fig. 5: Simulated output voltage for changing conditions. In blue, I_{ph} is kept constant while changing R_L. The opposite is shown in red.

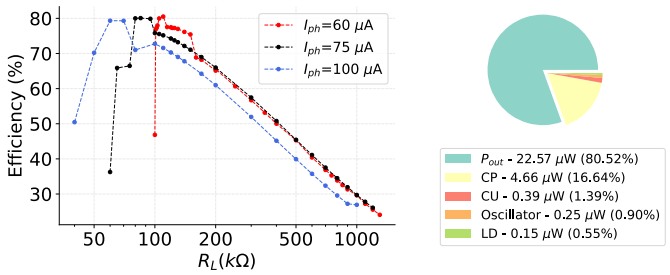

(a) (b)

Fig. 6: (a) Efficiency in terms of the load resistance. (b) Detailed description of the power consumption of each block.

show that this perturbation is not beneficial and the algorithm takes two steps backward. This results in the system oscillating around its optimum value (oscillations around 000100 in Fig. 4, of frequency 550 kHz).

Working at the MPP when $I_{ph} = 60$ μA would imply an input voltage equal to 0.647 V for the specific model of the photodiode used in simulation. However, for the particular case depicted in Fig. 4 with $R_L = 170$ kΩ, the simulated response of the proposed system determined that the point of operation that maximizes the output power corresponds to an input voltage of 0.684 V. For this particular case, working at the MPP of the photodiode would mean using a very high frequency, which would degrade the performance of the charge pump. Besides, having a higher input voltage reduces the on-resistance of the switching transistors (higher overdrive voltages). Depending on R_L, the optimum operating point varies, but generally it does not have to match with the MPP of the photodiode.

The proposed system is able to converge into an optimal solution regardless of the changes in the input and output conditions. The action of the algorithm varying the load resistance and the illuminance over time can be seen in Fig. 5. In each case, the system finds the operating frequency where the output power is maximized and remains around it.

The power efficiency of the system is evaluated varying R_L for several values of I_{ph} and the results are shown in Fig. 6a. Under these conditions, the harvester achieves a peak efficiency of 80.51% when $R_L = 110$ kΩ and $I_{ph} = 60$ μA, delivering an output power of 22.56 μW. The power consumption of the constituent blocks of the system is shown in Fig. 6b. The most power hungry block is the charge pump (16.64%), followed by the digital control unit (1.39%), the oscillator (0.9%), and finally, the level detectors (0.27%).

V. Conclusions

In this paper it has been shown that, when implementing a MPPT algorithm in a photovoltaic energy harvesting circuit, it results beneficial to perform the tracking of the output power instead of forcing the circuit's operation to the point of maximum photogenerated power. A circuit that uses this approach was implemented and electrical simulations show that it is able to maximize its output power, achieving a peak efficiency of 80.51% for an input power equal to 28.03 μW. The study of the region of operation of the electrical simulated results shows as well that the point that yields the maximum output power does not necessarily have to coincide on the MPP of the photovoltaic transducer.

References

[1] J. Zhao *et al.*, "Photovoltaic power harvesting technologies in biomedical implantable devices considering the optimal location," *IEEE J. Electromagn., RF, Microw. Med. Biol.*, vol. 4, no. 2, pp. 148–155, 2020.

[2] S. Roy *et al.*, "Powering solutions for biomedical sensors and implants inside the human body: A comprehensive review on energy harvesting units, energy storage, and wireless power transfer techniques," *IEEE Trans. Power Electron.*, vol. 37, no. 10, pp. 12 237–12 263, 2022.

[3] R. Vullers, R. van Schaijk *et al.*, "Micropower energy harvesting," *Solid-State Electronics*, vol. 53, no. 7, pp. 684–693, 2009.

[4] G. Chen *et al.*, "A cubic-millimeter energy-autonomous wireless intraocular pressure monitor," in *2011 IEEE International Solid-State Circuits Conference*, 2011, pp. 310–312.

[5] S. Ayazian *et al.*, "A photovoltaic-driven and energy-autonomous cmos implantable sensor," *IEEE Trans. Biomed. Circuits Syst.*, vol. 6, no. 4, pp. 336–343, 2012.

[6] T. Esram and P. L. Chapman, "Comparison of photovoltaic array Maximum Power Point Tracking techniques," *IEEE Trans. Energy Convers.*, vol. 22, no. 2, pp. 439–449, 2007.

[7] P. Favrat *et al.*, "A high-efficiency CMOS voltage doubler," *IEEE J. Solid-State Circuits*, vol. 33, no. 3, pp. 410–416, 1998.

[8] D. Cotfas *et al.*, "Methods to determine the dc parameters of solar cells: A critical review," *Renewable and Sustainable Energy Reviews*, vol. 28, pp. 588–596, 2013.

[9] K. Rawy *et al.*, "An 88% efficiency 0.1–300-μW energy harvesting system with 3-D MPPT using switch width modulation for iot smart nodes," *IEEE J. Solid-State Circuits*, vol. 53, no. 10, pp. 2751–2762, 2018.

[10] O. Pereira-Rial *et al.*, "Ultra-low-power low-input-voltage charge pump for micro-energy harvesting applications," *IEEE Trans. Circuits Syst. I, Reg. Papers*, vol. 70, no. 1, pp. 154–165, 2023.

[11] A. Ballo *et al.*, "Optimized charge pump with clock booster for reduced rise time or silicon area," *IEEE Trans. Circuits Syst., II, Exp. Briefs*, vol. 66, no. 12, pp. 1977–1981, 2019.

[12] S. Dai and J. K. Rosenstein, "A 14.4nW 122KHz dual-phase current-mode relaxation oscillator for near-zero-power sensors," *2015 IEEE Custom Integrated Circuits Conference (CICC)*, pp. 1–4, 2015.

[13] S. Babayan-Mashhadi and R. Lotfi, "Analysis and design of a low-voltage low-power double-tail comparator," *IEEE Trans. Very Large Scale Integr. (VLSI) Syst.*, vol. 22, no. 2, pp. 343–352, 2014.

[14] P.-H. Chen, K. Ishida, K. Ikeuchi *et al.*, "Startup techniques for 95 mV step-up converter by capacitor pass-on scheme and v_{th}-tuned oscillator with fixed charge programming," *IEEE J. Solid-State Circuits*, vol. 47, no. 5, pp. 1252–1260, 2012.